Towards Accurate Medical Image Segmentation With Gradient-Optimized Dice Loss

Qi Ming and Xiaowu Xiao

***Abstract*—Medical image segmentation plays an important role in medical diagnosis, and has received extensive attention in recent years. A large number of convolutional neural network based methods have been proposed to achieve accurate segmentation results. Dice loss is the most popular loss function for medical image segmentation tasks. However, we found that Dice loss suffers from abnormal gradient changes, which causes the loss function to be unstable and difficult to converge. Therefore, we propose an gradient-optimized Dice loss (GODC) to solve this problem. GODC corrects the abnormal gradient changes in the segmentation loss, which accelerates the model convergence and can achieve better segmentation performance. Next, we propose a lateral feature alignment module (LFAM). LFAM adopts deformable convolutional network to align the features of different layers on the shortcut connections of U-Net to improve the segmentation performance. Finally, our method achieves state-of-the-art results on the LiTS dataset as well as our collected pancreatic tumor datasets.**

***Index Terms*—Medical image segmentation, dice loss, convolutional neural network, gradient descent algorithm.**

I. Introduction

THE liver and pancreas play very important roles in the metabolism of the human body. Therefore, efficient diagnosis of liver tumors and pancreatic tumors is very important for medical image analysis. The rise of computerized tomography (CT) technology provides an effective way for tumor segmentation, which has been widely used in medical diagnosis. However, tumor lesions and surrounding tissues are extremely similar and difficult to distinguish. Many previous hand-crafted segmentation methods cannot achieve accurate medical image segmentation performance [1], [2], [3].

In recent years, a large number of methods based on convolutional neural networks have emerged, which have greatly improved the accuracy of medical image segmentation [4], [5], [6]. The powerful ability of CNN to automatically extract features endows the model with better segmentation performance. However, CNN-based segmentation methods also bring many problems.

Manuscript received 2 September 2023; revised 23 October 2023; accepted 25 October 2023. Date of publication 1 November 2023; date of current version 9 January 2024. This work was supported by the IEEE Publication Technology Department. The associate editor coordinating the review of this manuscript and approving it for publication was Dr. Aiping Liu. *(Corresponding author: Xiaowu Xiao.)*

Qi Ming is with the School of Automation, Beijing Institute of Technology, Beijing 100081, China (e-mail: chaser.ming@gmail.com).

Xiaowu Xiao is with the School of Information Resource Management, Liaoning University, Shenyang 110036, China (e-mail: xxw200999@163.com).

Digital Object Identifier 10.1109/LSP.2023.3329437

Currently the most popular loss function for segmentation is Dice loss [7], [8], [9], [10], [11]. However, we found that Dice loss suffers from abnormal gradient changes during the training process. Firstly, the gradients of the Dice loss increase as the model converges, which leads to oscillations in the loss curve and hinders further model convergence. Secondly, for large lesions, Dice loss produces smaller gradients. As a result, it produces a small step for parameter updation and therefore leads to slower convergence for large lesions.

U-Net [12] is a widely used model for medical image segmentation and achieves high-quality segmentation performance. Many of the existing advanced segmentation models are based on the U-Net framework [13], [14], [15]. U-Net employs downsampling and upsampling operations to extract symmetric feature maps. The corresponding features are then fused using a lateral connection path for subsequent segmentation prediction. However, we suggest that the feature maps obtained after downsampling and upsampling cannot be directly aligned with the original feature maps. Therefore, it is not feasible to directly concatenate different features. The semantic gap between these feature maps would make the fused feature with confusing semantic information.

Another problem stems from the available medical image data. Although CNN-based models are able to extract high-quality features to improve segmentation accuracy, a sufficient amount of data is still required to feed CNN models to achieve high segmentation performance. However, the available medical image data for liver and pancreas is very small, which makes it impossible to build a complete dataset for identification of various lesions. Insufficient data for different special cases will hinder model training and convergence.

To address the above issues, we optimize the existing segmentation framework. First, we design a gradient-optimized Dice loss (GODC) to eliminate the gradient instability problem of the classical Dice loss during training. GODC eliminates abnormal gradient changes in the classical Dice loss, thereby speeding up the training process and ensuring better segmentation performance. Then, the variability convolution is applied to the shortcut connection of U-Net to achieve feature alignment of feature maps and alleviate the semantic gap between different features.

Moreover, pancreatic cancer is one of the major problems that threatens human health and urgently needs to be addressed. Fast and accurate diagnosis of early pancreatic tumors helps to reduce the risk of cancer by early intervention. Medical image segmentation techniques based on deep learning can make a

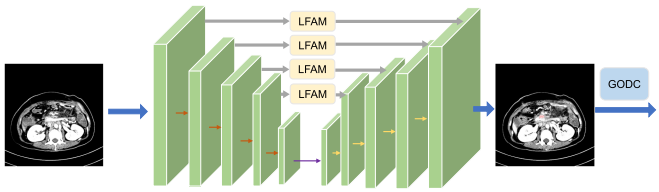

Fig. 1. The overall framework of the proposed method. GODC denotes the gradient-optimized Dice loss.

big difference in this field. For this purpose, we collected a pancreatic tumor segmentation dataset for the development of this field.

In summary, the contributions in this paper are as follows:

- We observe undesirable gradient changes of classical Dice loss during the training process. On this basis, a gradient-optimized Dice loss is proposed to achieve better segmentation performance.
- To bridge the semantic gap in feature fusion for U-Net based frameworks, we propose a lateral feature alignment module to spatially align features for further fusion process. In this way, the extracted features contain richer semantic information, which is beneficial to the subsequent segmentations.
- A pancreatic tumor segmentation dataset is constructed to further help address pancreatic cancer diagnosis. The proposed method also achieves superior performance on it.

II. Methodology

Dice loss is a very popular loss function in medical image segmentation. Given the input image $\mathcal{I}$, $V = \{1, 2, ..., n\}$ represents all pixels in $\mathcal{I}$. We denote G as the pixel-wise ground-truth (GT) labels for $\mathcal{I}$. $G \in \{0, 1\}^V$, in which 0 denotes the background pixesl and 1 for GT mask. Then, P is the output probabilities of the network for pixel-wise image segmentation task, and $P = \{p_0, p_1, \ldots, p_n\}$. Next, the intersection and union between predicted mask and the GT mask is as follows:

$$\begin{cases} I(P,G) = \sum_{v \in V} P_v * G_v, \\ U(P,G) = \sum_{v \in V} P_v + G_v - P_v * G_v, \end{cases} \tag{1}$$

where $I(P,G)$ means the overlap between two regions and $U(P,G)$ is the union area of them. The Dice similarity coefficient is organized as follows:

$$DC(P,G) = \frac{2 \cdot I(P,G)}{I(P,G) + U(P,G)} \tag{2}$$

The result in (2) is similar to a popular metric IoU in object detection, which is as follows:

$$IoU(P,G) = \frac{I(P,G)}{U(P,G)}. \tag{3}$$

IoU, as a common indicator for object detection [16], [17], [18], can directly reflect the spatial overlap between two regions. IoU is also usually used as an evaluation metric for segmentation tasks [19], [20], [21].

Obviously, we can get the relation between the Dice and IoU as follows:

$$DC(P,G) = \frac{2 \cdot IoU(P,G)}{1 + IoU(P,G)} \tag{4}$$

In order to analyze the gradient change of the Dice loss, we can first analyze the gradient change of IoU w.r.t. the prediction results during the training process [21]. The gradient of the IoU item w.r.t. the network outputs is as follows:

$$\begin{aligned} \frac{\partial IoU}{\partial P_v} &= \frac{\partial}{\partial P_v}\left[\frac{I}{U}\right] \\ &= \frac{1}{U^2} \cdot \left(U \cdot \frac{\partial I}{\partial P_v} - I \cdot \frac{\partial U}{\partial P_v}\right) \\ &= \frac{1}{U^2} \cdot \left[U \cdot Y_v - I \cdot (1 - Y_v)\right], \end{aligned} \tag{5}$$

in which I and U are intersection and union in (1), respectively. The general Dice loss is as follows:

$$L_{DC} = 1 - DC(P,G). \tag{6}$$

Combined (4), (5), and (6), we get the gradient of the Dice loss w.r.t. the predictions as follows:

$$\begin{aligned} \frac{\partial L_{DC}}{\partial P_v} &= -\frac{\partial DC}{\partial P_v} \\ &= -\frac{\partial DC}{\partial IoU} \cdot \frac{\partial IoU}{\partial P_v} \\ &= -\frac{2 \cdot Y_v - IoU \cdot (1 - Y_v)}{(1 + IoU)^2 \cdot U} \end{aligned} \tag{7}$$

The result of (7) show that the gradient of Dice loss is inversely proportional to the union area between the predicted mask and GT mask. It leads to the following problems: (1). Once the training model predicts a large mask initially, a small gradient would be obtained and it is difficult to quickly optimize the model parameters. As a result, the model would suffer from slow convergence. (2) As the optimization proceeds, a small GT mask produces a relatively small union area, which would lead to a large gradient. It's hard to refine the prediction mask next to achieve accurate segmentation results in this case.

Therefore, we expect Dice loss to achieve a scale-invariant optimization process to avoid the suboptimal training process caused by the above issues. Then the gradient scaling strategy is applied to construct the Gradient-Optimized Dice Loss (GODC) as follows:

$$L_{DC} = (1 - DC(P,G)) \cdot ||U||^*. \tag{8}$$

$||U||^*$ is the norm of the union vector normalized within a batch. The modification of GCOD is small based on Dice loss, but the performance gain is substantial. In (I), we achieve a scale-independent optimization process by adaptively scaling gradients with the union area. The gradient of the loss function could also be positively related to the object scales if we multiply $(||U||^*)^2$ on Dice loss. Although it helps to further speed up model convergence, we suggest that the unstable mask predictions of the segmentation task in the early stages of training may

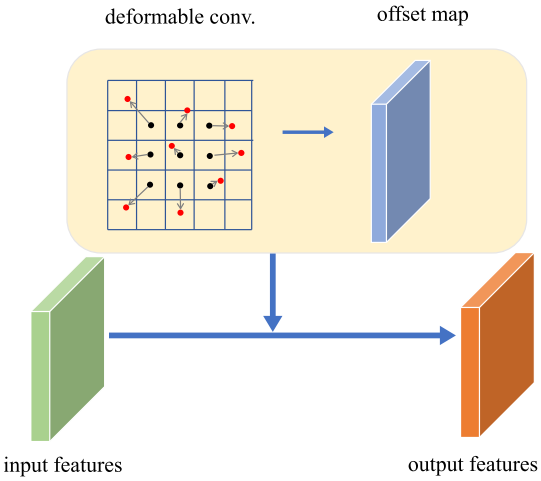

Fig. 2. Illustration of the lateral feature alignment module. Deformable convolutions are applied in lateral connections to achieve feature alignment between the two features to be fused.

cause severe loss oscillations. Hence the design in (1) achieves a better trade-off between performance and convergence speed.

Most of the current medical image segmentation frameworks are inherited from UNet. These methods firstly use downsampling modules to obtain small-scale feature maps, and then upsample and restore large-scale feature maps for subsequent fine-grained segmentation tasks [22], [23]. However, the padding operations introduce quantization error, which would cause the feature map to be spatially biased from the features of the original image. Besides, fusion of not aligned features would make the semantic information of the near region ambiguous and hard to distinguish. It degrades the performance especially for small-scale tumor regions. Hence, subsequent segmentation based on misaligned features would inevitably lead to inaccurate segmentation results.

We observed that the translation error caused by padding is not too large, and we only need to fine-tune the position of the feature maps during the feature fusion procedure. Therefore, a lateral feature alignment module (LFAM) is proposed. LFAM introduces deformable convolution blocks [24] to achieve the adaptive fusion of corresponding features at the same scales. The structure is shown in the Fig. 2. Unlike traditional convolutional kernels, deformable convolutional kernels use learnable convolutional layers to locate sampling points. It helps to solve the feature misalignment problem in lateral connections.

III. Experiments and Analysis

A. Datasets

We evaluate the performance of the proposed method on two datasets. The MICCAI 2017 Liver Tumor Segmentation (LiTS) Challenge [25] dataset contains 201 CT scans, including 131 scans for training and 70 scans for testing. The data and segmentations are provided by various clinical sites around the world. Further, we collected a pancreatic tumor segmentation dataset to assist in the fast and accurate diagnosis of pancreatic cancer. The datasets were collected from different institutions, and the patient's consent is also obtained for academic research. It contains a total of 174 scans. Specifically, the dataset is divided into 140 scans as a training set and 34 scans for testing.

B. Evaluate Metric

We adopted the most commonly used Dice coefficient to evaluate the performance of the models, which is as follows:

$$\text{Dice} = \frac{2 \cdot TP}{2TP + FN + FP} \tag{9}$$

in which TP, FP and FN are the number of pixels in the predicted mask that are true positives, false positives and false negatives, respectively. The Dice coefficient is similar to the IoU metric as we discussed in previous section. A higher dice coefficient means the more spatial overlap between the prediction mask and the GT label, and therefore the prediction is more accurate. Also, we adopt precision and recall to evaluate the models, which are defined as follows:

$$\text{Precision} = \frac{TP}{TP + FP} \tag{10}$$

$$\text{Recall} = \frac{TP}{TP + FN} \tag{11}$$

Precision is the ratio of true positive sample among all positive prediction. Recall reveals the accuracy of positive predictions among all true positives.

C. Implementation Details

Our implementation is based on the open source framework PyTorch [27]. In the data augmentation process, we set the random scaling factor in $[0.7, 1.3]$ and the random translation ranges in $[0.8, 1.2]$. Images are randomly rotated by 90°. We train the model on RTX 2080 Ti GPU. Five-fold cross-validation is adopted during training. We use the Adam optimizer to train the model with the learning rate set to 2×10^{-4}. The model is trained for 1000 epochs with a batchsize set to 2. All ablation experiments are performed on our collected pancreatic tumor segmentation dataset. Finally, we compare with other methods on the public LiTS dataset.

D. Ablation Study

We conducted extensive ablation experiments on the collected pancreatic tumor segmentation dataset to prove the effectiveness of the proposed method. The modules we propose are all plug-gable structures, which can be easily applied to existing models to achieve performance improvements. Next, we will conduct detailed experiments on each module.

1) Effectiveness of Gradient-Optimized Dice Loss: GODC solves the abnormal gradient change of Dice loss, and therefore it helps to speed up the model convergence and improve the segmentation performance. GODC improves the performance of U-Net by 1.3% with only slight changes to the original Dice loss. To further prove the generality of the proposed method, we also conduct experiments on other models. The results in

TABLE I
EVALUATION OF GRADIENT-OPTIMIZED DICE LOSS ON DIFFERENT MODELS ON PANCREATIC TUMOR DATASET

Model	Training loss	Dice(%)
U-Net[12]	DC	67.6
	GODC	68.9
Residual U-Net[26]	DC	68.2
	GODC	69.1

DC is the Dice loss, and GODC denotes gradient-optimized Dice loss.

TABLE II
EVALUATION OF LATERAL FEATURE ALIGNMENT MODULE (LFAM) ON PANCREATIC TUMOR DATASET

Model	LFAM	Conv. Shared	Dice(%)
U-Net[12]	×	–	67.6
	✓	×	68.3
	✓	✓	68.0
Residual U-Net[26]	×	–	68.2
	✓	×	68.6
	✓	✓	68.5

'Conv. shared' means sharing the deformable convolution kernels in LFAMs among fetures with different scales.

Table I show that with the application of GODC, the Dice index of Residual U-Net [26] is improved by 0.9 points in the pancreatic tumor segmentation task. GODC helps to improve the performance of existing segmentation frameworks with little additional computational overhead.

2) Effectiveness of Lateral Feature Alignment Module: Lateral connections are essential in UNet-based models. Our proposed LFAM effectively alleviates the misalignment between fusion features and achieve performance improvement. LFAM bridges feature maps at different scales, which is similar to the multi-scale feature pyramid network (FPN) in object detection [28]. In FPN, it is reported that the convolutional kernels with shared parameters between feature maps of different scales can enhance the generalization ability of the model. Therefore we also tried shared deformable convolutional kernels in LFAM. Experiments are performed on U-Net and Residual U-Net. The results are shown in Table II. The performance achieved by the shared convolutional kernels is inferior to independent convolutional kernels. We suggest that shared convolutional kernels expect to extract more robust feature representations from features of different scales to achieve scale invariance. On the one hand, the shared parameters make it difficult for the convolutional kernels to converge well. On the other hand, the scale-sensitive position offset provided by LFAM is better to solve the spatial misalignment between feature maps. Therefore, we adopt independent convolutions in LFAM. Finally, LFAM improves U-Net and Residual U-Net by 0.7% and 0.4%, respectively.

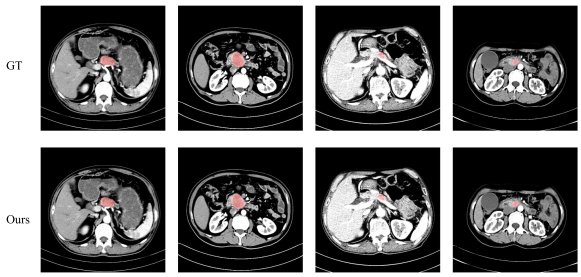

Fig. 3. Segmentation results of our method on the pancreatic tumor dataset. The first row is the GT annotation and the second row is the segmentation mask of our method.

TABLE III
COMPARISON WITH OTHER ADVANCED METHODS ON THE LITS LIVER SEGMENTATION DATASET

Method	Dice(%)	Precision(%)	Recall(%)
U-Net[12]	91.21	89.99	92.79
ResUNet[29]	92.29	93.30	93.58
U-Net++[30]	93.06	93.98	94.02
Attention U-Net[31]	93.07	94.65	94.74
CE-Net[32]	94.39	95.72	95.76
DFS U-Net[33]	94.93	93.56	91.79
MSN-Net[34]	94.24	92.87	93.42
Ours	**95.32**	**96.79**	**96.01**

Some visualization results are shown in Fig. 3. We visualize images with tumor regions of different sizes and shapes and their corresponding segmentation results. It can be seen that our model can accurately segment the tumor area.

E. Comparison With Other Methods

We conduct experiments on the publicly available LiTS liver segmentation dataset and report the comparison results with other advanced methods in Table III. Our method achieves the best performance with Dice index of 95.32%, precision of 96.79%, and recall of 96.01%. We did not perform extensive modification of the baseline model, but the segmentation performance surpassed many recent models. Furthermore, notice that our proposed method is very flexible and requires only minor adjustments to existing models. Therefore, applying our method to other models can also achieve continuous improvement.

IV. CONCLUSION

In this paper, we first analyze the gradient change of the current popular Dice loss. Based on the observation, a gradient-optimized Dice (GODC) loss is proposed to achieve fast and stable model convergence. Next, we introduce lateral feature alignment module (LFAM) in the lateral connection and feature fusion steps. LFAM employs deformable convolutions to achieve spatial alignment of the features to be fused, which helps to eliminate the semantic gap between the misaligned feature maps. Finally, the superior performance on the LiTS dataset and the collected pancreatic cancer dataset prove the effectiveness of our method.

REFERENCES

[1] F. Lu, F. Wu, P. Hu, Z. Peng, and D. Kong, "Automatic 3D liver location and segmentation via convolutional neural network and graph cut," *Int. J. Comput. Assist. Radiol. Surg.*, vol. 12, no. 2, pp. 171–182, 2017.

[2] O. F. Abd-Elaziz, M. S. Sayed, and M. I. Abdullah, "Liver tumors segmentation from abdominal CT images using region growing and morphological processing," in *Proc. IEEE Int. Conf. Eng. Technol.*, 2014, pp. 1–6.

[3] A. M. Anter and A. E. Hassenian, "CT liver tumor segmentation hybrid approach using neutrosophic sets, fast fuzzy c-means and adaptive watershed algorithm," *Artif. Intell. Med.*, vol. 97, pp. 105–117, 2019.

[4] Y. Lang et al., "Localization of craniomaxillofacial landmarks on CBCT images using 3D mask R-CNN and local dependency learning," *IEEE Trans. Med. Imag.*, vol. 41, no. 10, pp. 2856–2866, Oct. 2022.

[5] R. Zheng et al., "Automatic liver tumor segmentation on dynamic contrast enhanced MRI using 4D information: Deep learning model based on 3D convolution and convolutional LSTM," *IEEE Trans. Med. Imag.*, vol. 41, no. 10, pp. 2965–2976, Oct. 2022.

[6] Y. Zhang et al., "3D multi-attention guided multi-task learning network for automatic gastric tumor segmentation and lymph node classification," *IEEE Trans. Med. Imag.*, vol. 40, no. 6, pp. 1618–1631, Jun. 2021.

[7] Y.-C. Liu, D. S. Tan, J.-C. Chen, W.-H. Cheng, and K.-L. Hua, "Segmenting hepatic lesions using residual attention U-Net with an adaptive weighted dice loss," in *Proc. IEEE Int. Conf. Image Process.*, 2019, pp. 3322–3326.

[8] J. Chi, X. Han, C. Wu, H. Wang, and P. Ji, "X-Net: Multi-branch unet-like network for liver and tumor segmentation from 3D abdominal CT scans," *Neurocomputing*, vol. 459, pp. 81–96, 2021.

[9] L. Zhou, X. Deng, W. Li, S. Zheng, and B. Lei, "A contour-aware feature-merged network for liver segmentation based on shape prior knowledge," *Neurocomputing*, vol. 457, pp. 389–399, 2021.

[10] N. Altini et al., "Liver, kidney and spleen segmentation from CT scans and mri with deep learning: A survey," *Neurocomputing*, vol. 490, pp. 30–53, 2022.

[11] V. Czipczer and A. Manno-Kovacs, "Adaptable volumetric liver segmentation model for CT images using region-based features and convolutional neural network," *Neurocomputing*, vol. 505, pp. 388–401, 2022.

[12] O. Ronneberger, P. Fischer, and T. Brox, "U-Net: Convolutional networks for biomedical image segmentation," in *Proc. Int. Conf. Med. Image Comput. Comput.- Assist. Intervention*, 2015, pp. 234–241.

[13] J. Zhang, J. Zeng, P. Qin, and L. Zhao, "Brain tumor segmentation of multi-modality MR images via triple intersecting U-Nets," *Neurocomputing*, vol. 421, pp. 195–209, 2021.

[14] C. Zhu et al., "Multi-level colonoscopy malignant tissue detection with adversarial cac-unet," *Neurocomputing*, vol. 438, pp. 165–183, 2021.

[15] M. Lin, Q. Cai, and J. Zhou, "3D MD-UNet: A novel model of multi-dataset collaboration for medical image segmentation," *Neurocomputing*, vol. 492, pp. 530–544, 2022.

[16] Q. Ming, Z. Zhou, L. Miao, H. Zhang, and L. Li, "Dynamic anchor learning for arbitrary-oriented object detection," in *Proc. AAAI Conf. Artif. Intell.*, 2021, pp. 2355–2363.

[17] Q. Ming, L. Miao, Z. Zhou, and Y. Dong, "CFC-Net: A critical feature capturing network for arbitrary-oriented object detection in remote-sensing images," *IEEE Trans. Geosci. Remote Sens.*, vol. 60, 2022, Art. no. 5605814.

[18] J. Yu, Y. Jiang, Z. Wang, Z. Cao, and T. Huang, "Unitbox: An advanced object detection network," in *Proc. 24th ACM Int. Conf. Multimedia*, 2016, pp. 516–520.

[19] D. Bolya, C. Zhou, F. Xiao, and Y. J. Lee, "YOLACT: Real-time instance segmentation," in *Proc. IEEE/CVF Int. Conf. Comput. Vis.*, 2019, pp. 9157–9166.

[20] C. Yu, J. Wang, C. Peng, C. Gao, G. Yu, and N. Sang, "BiseNet: Bilateral segmentation network for real-time semantic segmentation," in *Proc. Eur. Conf. Comput. Vis.*, 2018, pp. 325–341.

[21] M. A. Rahman and Y. Wang, "Optimizing intersection-over-union in deep neural networks for image segmentation," in *Proc. Int. Symp. Vis. Comput.*, 2016, pp. 234–244.

[22] Y. Zhou, W. Huang, P. Dong, Y. Xia, and S. Wang, "D-UNet: A dimension-fusion U shape network for chronic Stroke Lesion Segmentation," *IEEE/ACM Trans. Comput. Biol. Bioinf.*, vol. 18, no. 3, pp. 940–950, May/Jun. 2021.

[23] B. Baheti, S. Innani, S. Gajre, and S. Talbar, "EFF-UNet: A novel architecture for semantic segmentation in unstructured environment," in *Proc. IEEE/CVF Conf. Comput. Vis. Pattern Recognit. Workshops*, 2020, pp. 358–359.

[24] J. Dai et al., "Deformable convolutional networks," in *Proc. IEEE Int. Conf. Comput. Vis.*, 2017, pp. 764–773.

[25] P. Bilic et al., "The liver tumor segmentation benchmark (lits)," *Med. Image Anal.*, vol. 84, 2023, Art. no. 102680.

[26] Z. Zhang, Q. Liu, and Y. Wang, "Road extraction by deep residual U-Net," *IEEE Geosci. Remote Sens. Lett.*, vol. 15, no. 5, pp. 749–753, May 2018.

[27] A. Paszke et al., "Pytorch: An imperative style, high-performance deep learning library," in *Proc. Adv. Neural Inf. Process. Syst.*, vol. 32, 2019, pp. 8024–8035.

[28] T.-Y. Lin, P. Dollár, R. Girshick, K. He, B. Hariharan, and S. Belongie, "Feature pyramid networks for object detection," in *Proc. IEEE Conf. Comput. Vis. Pattern Recognit.*, 2017, pp. 2117–2125.

[29] X. Han, "Automatic liver lesion segmentation using a deep convolutional neural network method," 2017, *arXiv:1704.07239*.

[30] Z. Zhou, M. M. R. Siddiquee, N. Tajbakhsh, and J. Liang, "UNet : A nested U-Net architecture for medical image segmentation," in *Deep Learning in Medical Image Analysis and Multimodal Learning for Clinical Decision Support*. Berlin, Germany: Springer, 2018, pp. 3–11.

[31] O. Oktay et al., "Attention U-Net: Learning where to look for the pancreas," 2018, *arXiv:1804.03999*.

[32] Z. Gu et al., "CE-Net: Context encoder network for 2D medical image segmentation," *IEEE Trans. Med. Imag.*, vol. 38, no. 10, pp. 2281–2292, Oct. 2019.

[33] Z. Liu et al., "Automatic liver segmentation from abdominal ct volumes using improved convolution neural networks," *Multimedia Syst.*, vol. 27, no. 1, pp. 111–124, 2021.

[34] T. Fan, G. Wang, X. Wang, Y. Li, and H. Wang, "MSN-Net: A multi-scale context nested U-Net for liver segmentation," *Signal, Image Video Process.*, vol. 15, no. 6, pp. 1089–1097, 2021.